ACS Sustainable Chemistry & Engineering

Research Article

pubs.acs.org/journal/ascecg

Activated Carbon-Coated Carbon Nanotubes for Energy Storage in Supercapacitors and Capacitive Water Purification

Kaiyuan Shi, Meng Ren, and Igor Zhitomirsky*

Department of Materials Science and Engineering, McMaster University, 1280 Main Street West, Hamilton, Ontario, Canada L8S 4L7

Supporting Information

ABSTRACT: Polypyrrole-coated multiwalled carbon nanotubes (PPy-MWCNT) were used for the fabrication of activated carbon-coated MWCNT doped with nitrogen (N-AC-MWCNT). The conceptually new method for the fabrication of non-agglomerated PPy-MWCNT with good coating uniformity allowed the fabrication of uniform and well-dispersed N-AC-MWCNT with high surface area. The use of N-AC-MWCNT allowed the fabrication of supercapacitor electrodes with high mass loading in the range of 15−35 mg cm^{-2} and with a high active material to current collector mass ratio of 0.21−0.50. The N-AC-MWCNT electrodes showed excellent electrochemical performance in aqueous 0.5 M Na_2SO_4 electrolyte. The maximum specific capacitance of 3.6 F cm^{-2} (103.1 F g^{-1}) was achieved for mass loading of 35 mg cm^{-2} at a scan rate of 2 mV s^{-1}. The aqueous supercapacitor cells, based on N-AC-MWCNT electrodes, exhibited excellent performance with energy density of 16.1 mWh g^{-1}, power density of 14.4 W g^{-1}, and enlarged voltage window of 1.8 V. The individual electrodes and cells showed good capacitance retention at high charge−discharge rates and good cycling stability. Moreover, the N-AC-MWCNT electrodes showed promising performance for capacitive deionization of water. The feasibility of capacitive removal of organic dyes from aqueous solutions has been demonstrated. A quartz crystal microbalance method was used as a tool for the analysis of electrosorption and electrodesorption of ions and charged dyes during charge and discharge.

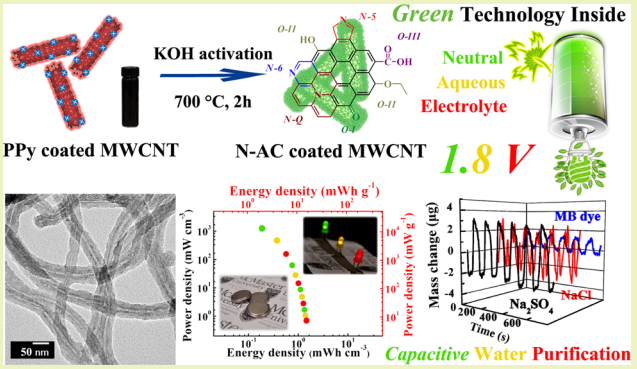

KEYWORDS: *Supercapacitor, Activated carbon, Carbon nanotube, Capacitive deionization, Dye, Polypyrrole*

INTRODUCTION

Carbon materials, such as carbon nanotubes, graphene, and activated carbon, are currently under intensive investigations for energy storage in electrochemical supercapacitors.[1−3] Many studies were focused on the development of materials and composites with high capacitance, large voltage windows, low impedance, and good cycling stability.[4,5] Considerable attention has been given to the development of efficient electrodes with high mass loading of active materials and high active material to current collector mass ratios.[6]

Carbon-based supercapacitors, containing organic electrolytes, offer the advantage of large voltage windows, which allows high energy density.[7] However, some organic electrolytes are relatively expensive, toxic, and flammable. Moreover, carbon electrodes showed reduced capacitance and increased impedance in organic electrolytes. On the basis of this consideration, many efforts have been made to increase the voltage window of carbon-based supercapacitors using environmentally friendly, cost-effective, and safe aqueous electrolytes.[7−9]

A new wave of interest in the development of aqueous supercapacitor devices, based on carbon materials, is attributed to their applications for capacitive deionization of water (CDI).[10−13] CDI is considered a green and economic desalination technology,[14] which involves the use of electric double-layer capacitors.[13,15−18] It was demonstrated that high deionization efficiency can be achieved using porous carbon electrodes with high specific capacitance. Significant interest has been generated in the use of carbon nanotube electrodes for ion-selective deionizaton.[19,20]

The use of carbon nanotubes[21,22] as an electrode material offers the advantages of high electronic conductivity and good capacitance retention at high charge−discharge rates. However, the specific capacitance of carbon nanotubes is lower than that of activated carbon. The interest in activated carbon materials[23−25] is attributed to their high surface area, which allows high specific capacitance. However, the electronic conductivity of activated carbon is lower than that of carbon nanotubes. The specific capacitance of activated carbon decreased with increasing mass loading due to low electronic conductivity. The problem was addressed by the development of composites,[24,26,27] containing activated carbon and conductive additives, such as carbon nanotubes. These studies

Received: February 19, 2014
Revised: April 8, 2014
Published: April 16, 2014

Scheme 1. Schematic Illustration of the Fabrication Method of N-AC-MWCNT

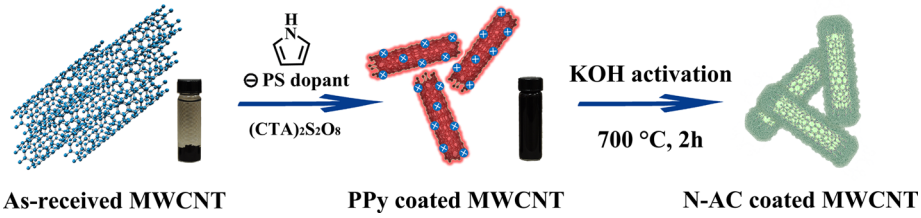

highlighted the importance of the optimization of the conductive additives content in the composites, good dispersion of the additives, and reduction of interface resistance.

Recent investigations showed that the capacitive behavior of carbon materials can be improved using various dopants, such as N and S.[28−30] It was found that the use of dopants resulted in higher electronic conductivity, improved wettability of the active materials by the electrolytes, and enhanced capacitance, attributed to the contribution of redox reactions[23] of the surface functional groups. Impressive progress[31−34] has been made in the development of doped carbons with controlled porosity and the investigation of the charge−discharge mechanism.

Significant interest has been generated in the use of N-enriched polymers as precursors for the fabrication of N-doped carbon materials by polymer carbonization methods. The use of N-enriched polymers allows the fabrication of advanced carbon materials with controlled N content. In contrast, carbon materials, produced from some natural precursors, suffer from the variation of their properties,[35] which is detrimental for practical applications in supercapacitors. Polypyrrole and polyaniline are important conductive polymer materials for the fabrication of N-doped carbons.[35−37] The use of polymers allowed the fabrication of activated carbon materials with ultrahigh specific surface area.[35] Investigations were also focused on the development of doped carbon nanotubes, nanowires, and nanosheets from polymer precursors.[38−41]

In the previous investigations,[42] a conceptually new approach has been developed for the fabrication of polypyrrole-coated multiwalled carbon nanotubes (PPy-MWCNT). The method allowed the fabrication of well-dispersed and uniformly coated MWCNT. The new approach paves the way for the fabrication of nitrogen-doped activated carbon-coated MWCNT (N-AC-MWCNT) with high surface area for application in efficient electrochemical devices.

The goal of this investigation was the fabrication of supercapacitor devices based on N-AC-MWCNT. The results presented below indicated that carbonization of PPy coatings and chemical activation allowed the fabrication of well-dispersed N-AC-MWCNT with high surface area. The use of MWCNT allowed good electronic conductivity and improved charge transfer. The important finding was the possibility of fabrication of electrodes with high capacitance at high mass loading, good capacitance retention at high scan rates, and good cyclic stability. The method allowed the fabrication of efficient electrochemical devices for energy storage with a voltage window of 1.8 V in an aqueous 0.5 M Na_2SO_4 electrolyte. Moreover, testing results indicated that N-AC-MWCNT are promising materials for CDI and capacitive dye removal (CDR) technologies. Compared to other dye removal technologies, such as photocatalytic degradation,[43−45] catalytic oxidation,[46] and adsorption,[47,48] CDR offers the advantage of simple regeneration of the active material and high efficiency.

EXPERIMENTAL PROCEDURES

Materials. Ponceau S (PS), cetrimonium bromide (CTAB), ammonium persulfate ($(NH_4)_2S_2O_8$), pyrrole (Py), potassium hydroxide (KOH), methyl blue (MB) dye, polyvinyl butyral (PVB), and polyvinylidene fluoride (PVDF) were obtained from Sigma-Aldrich. Py was stored in a refrigerator at 4 °C before the use. MWCNT were obtained from Arkema. Ni foam (95% porosity) was supplied by Vale.

Synthesis of PPy-Coated MWCNT. PPy-MWCNT were fabricated using oxidant−surfactant nanocrystals (Scheme 1), prepared by a chemical reaction between CTAB and $((NH_4)_2S_2O_8$ according to our previous study.[42] In a typical process, 0.3 g of MWCNT and 4.77 g of $(CTA)_2S_2O_8$ were mixed in 200 mL of deionized water and ultrasonicated for 1 h. The suspension was cooled to 4 °C, and then 200 mL of a solution containing 0.05 mol L^{-1} of Py and 0.015 mol L^{-1} PS was added. The reaction was performed at 4 °C for 20 h. Obtained material was washed with deionized water and dried at 70 °C in air.

Fabrication of Doped Carbon-Coated MWCNT. N-AC-MWCNT were prepared from PPy-MWCNT by a procedure (Scheme 1) that involved carbonization and chemical activation. Briefly, 2 g of PPy-MWCNT were dispersed in 50 mL of 4 mol L^{-1} KOH. The sedimentation tests showed good dispersibility of PPy-MWCNT in the KOH solution. The suspension was stable for more than one month. The prepared suspension was further stirred at 80 °C and dried. The obtained powder was carbonized in a tubular furnace under a nitrogen atmosphere at 700 °C for 2 h and then cooled to room temperature. The carbonized material was washed with 1 M HCl solution and then with deionized water until the filtrate became neutral. Obtained N-AC-MWCNT were dried in a vacuum oven at 90 °C overnight. For comparison, PPy-MWCNT were carbonized without KOH activation using a similar procedure to form N-doped carbon-coated MWCNT (N-C-MWCNT).

Fabrication of Electrodes and Cells. Supercapacitor electrodes were prepared by impregnation of Ni foam current collectors using suspensions of N-AC-MWCNT, N-C-MWCNT, and MWCNT in ethanol, containing 3 mass% of PVB binder. The active mass loading was varied in the range of 10−35 mg cm^{-2}. Two electrodes, separated by a porous membrane, were combined for the fabrication of coin cells (CR2032 type, MTI Corporation, U.S.A.), which were sealed using a hydraulic crimping machine (MSK-110, MTI Corporation, U.S.A.).

Characterization Methods. Electron microscopy investigations were performed using a transmission electron microscope (TEM, JEOL 2010F). X-ray photoelectron spectra (XPS) were recorded using a Physical Electronics (PHI) Quantera II spectrometer.

Electrochemical studies of individual electrodes in a three-electrode configuration and coin cells in a symmetrical two-electrode configuration were conducted using a potentiostat (PARSTAT 2273, Princeton Applied Research). The area of the individual working electrode was 1 cm^2. The counter electrode was platinum gauze, and the reference electrode was a standard calomel electrode (SCE). Capacitive behavior and electrochemical impedance of the electrodes were investigated in a neutral 0.5 M Na_2SO_4 aqueous electrolyte in a purified nitrogen gas atmosphere. Cyclic voltammetry (CV) studies were performed at scan rates of 2−200 mV s^{-1}. The capacitances of electrodes and cells $C = Q/\Delta V$ were calculated using half the integrated area of the CV curve to obtain the charge (Q) and subsequently dividing the charge by the width of the potential window (ΔV). The mass and area normalized capacitances, $C_m = C/m$ (m,

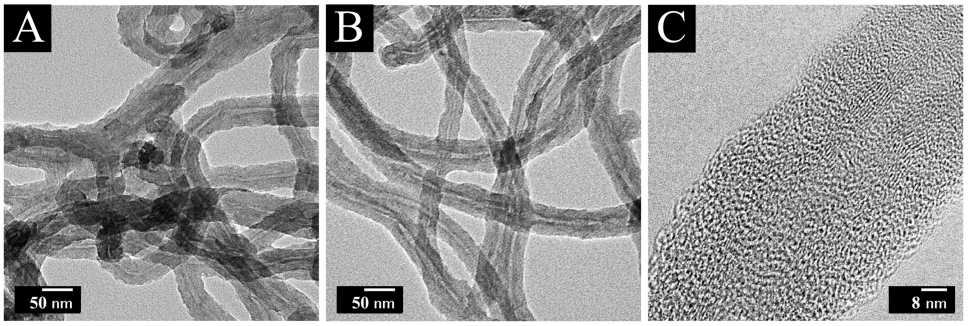

Figure 1. (A,B) TEM and (C) HRTEM images for (A) PPy-MWCNT and (B,C) N-AC-MWCNT.

Table 1. BET Surface Area, Total Porosity Volume (V_{total}), Microporosity (diameter <2 nm), Volume (V_{micro}), Average Pore Diameter, and Density of Investigated Materials

	BET surface area ($m^2\ g^{-1}$)	V_{total} ($cm^3\ g^{-1}$)	V_{micro} ($cm^3\ g^{-1}$)	average pore diameter (nm)	density ($g\ cm^{-3}$)
pristine MWCNT	325.48	0.24	0.09	5.32	0.72
N-C-MWCNT	489.39	0.37	0.11	6.23	0.68
N-AC-MWCNT	1889.12	1.72	0.61	3.78	0.24

active mass of electrode), $C_s = C/S$ (S, electrode area) of individual electrodes, and $C_{cm} = C_c/2m$, $C_{cs} = C_c/S$ of coin cells were analyzed. The alternating current (AC) complex impedance $Z^* = Z' - iZ''$ was analyzed in the frequency range from 10 mHz to 100 kHz at the amplitude of the AC signal of 5 mV. The complex capacitance[42] $C^* = C' - iC''$ was calculated from the impedance data as $C' = Z''/\omega|Z|^2$ and $C'' = Z'/\omega|Z|^2$, where $\omega = 2\pi f$, and f is the frequency. Charge–discharge behavior of the coin cells was investigated using a battery analyzer (BST8, MTI Corporation, U.S.A.).

Quartz crystal microbalance studies were performed using a microbalance (QCM 922, Princeton Applied Research) controlled by a computer. The mass changes of the quartz resonators were calculated using Sauerbrey's equation.[49,50] The electrochemical cell contained a Au-coated 9-MHz quartz resonator with an area of 0.2 cm^2 and a Pt counter electrode. The quartz resonators were coated using 1 μL of suspension, containing 20 mg of N-AC-MWCNT and 5% PVDF binder, dissolved in 1 mL of *N*-methylpyrrolidone. The suspension was cast on a resonator and dried in oven. The QCM studies were performed in the pulse mode, using positive and negative pulses with a constant voltage of 0.5 V.

RESULTS AND DISCUSSION

Figure 1 shows TEM images of PPy-MWCNT and N-AC-MWCNT. The use of non-agglomerated MWCNT, uniformly coated with PPy (Figure 1A), allowed the fabrication of non-agglomerated N-AC-MWCNT (Figure 1B). The analysis of HRTEM images (Figure 1C) showed that coating thickness was in the range of 12–15 nm. It was found (Figure S1, Supporting Information, Table 1) that specific surface area increased in the order of 325.5 (MWCNT), 489.4 (N-C-MWCNT), and 1889.1 $m^2\ g^{-1}$ (N-AC-MWCNT). The average pore diameter changed in the order of 5.32 (MWCNT), 6.23(N-C-MWCNT), and 3.78 nm (N-AC-MWCNT).

The XPS survey spectra of MWCNT and N-AC-MWCNT are shown in Figure 2A. The spectrum of N-AC-MWCNT revealed a N 1s peak. A weak S 1s peak in the spectrum of N-AC-MWCNT was observed due to the use of S-containing PS dye as an anionic dopant for PPy polymerization. The XPS data on chemical composition data are shown in Table S1 of the Supporting Information. The oxygen, nitrogen, and sulfur contents in N-AC-MWCNT were 7.89, 6.71, and 2.28 wt %, respectively. The high-resolution N 1s spectrum (Figure 2B) can be deconvoluted into three peaks located at 400.9, 399.8,

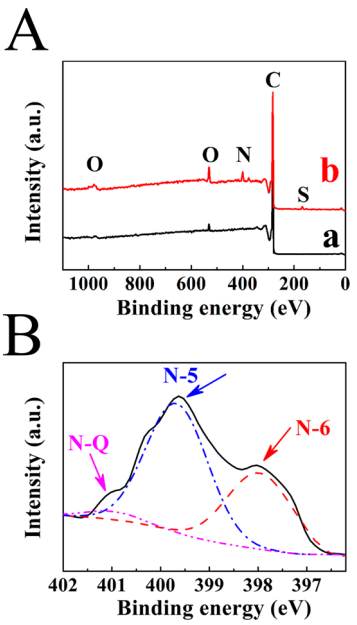

Figure 2. (A) Survey XPS spectra for (a) pristine MWCNT and (b) N-AC-MWCNT. (B) High-resolution XPS spectra for N 1s of N-AC-MWCNT, showing contributions of nitrogen-containing functional groups: N5 (pyrrole), N6 (pyridine), and N-Q (quaternary).

and 398.2 eV, which are attributed to quaternary (N-Q), pyrrolic (N-5), and pyridinic nitrogen (N-6) groups (Figure S2, Supporting Information), respectively.[51] It is known that the N-Q and N-6 groups have a stronger donor electron character, thus improving the electron transfer in supercapacitor electrodes at high current loads.[33] In addition, N-Q and N-5 nitrogens located at the edges of graphene layers enhanced the pseudocapacitance effect, wettability, and hydrophilicity of the electrode.[31] The analysis of XPS data revealed oxygen-containing groups (Figure S3, Supporting Information). The XRD and Raman spectroscopy data (Figures S4 and S5, Supporting Information) showed that N-AC-MWCNT have a low degree of graphitization. Sedimentation tests in the 0.5 M Na_2SO_4 aqueous electrolyte revealed significant improvement

dx.doi.org/10.1021/sc500118r | ACS Sustainable Chem. Eng. 2014, 2, 1289–1298

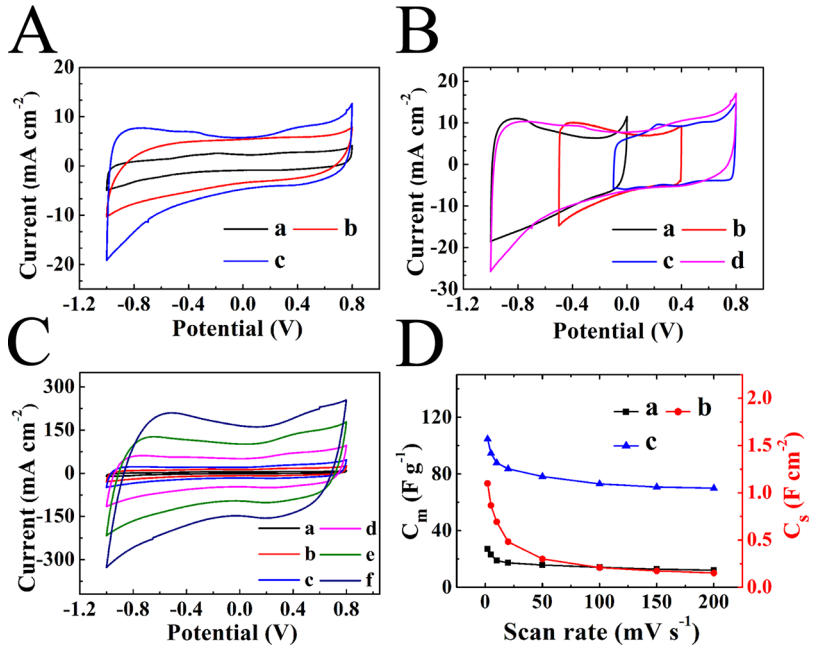

Figure 3. (A) CVs at a scan rate of 5 mV s^{-1} for (a) pristine MWCNT, (b) N-C-MWCNT, and (c) N-AC-MWCNT. (B) CVs for N-AC-MWCNT in voltage windows of (a) −1 to 0 V, (b) −0.5 to +0.4 V, (c) −0.1 to +0.8 V, and (d) −1 to +0.8 at a scan rate of 5 mV s^{-1}. (C) CVs for N-AC-MWCNT at scan rates of (a) 2, (b) 10, (c) 20, (d) 50, (e) 100, (f) 200 mV s^{-1}. (D) C_m and C_s versus scan rate for (a) pristine MWCNT, (b) N-C-MWCNT, and (c) N-AC-MWCNT. All electrodes have mass loadings of 15 mg cm^{-2}.

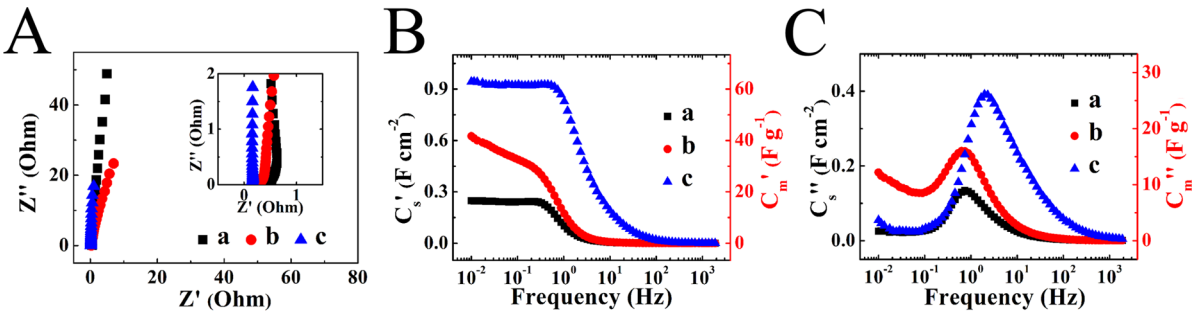

Figure 4. (A) Nyquist plot of complex impedance; inset shows high frequency range. (B) C_s' and C_m' and (C) C_s'' and C_m'' calculated from the impedance data versus frequency for (a) pristine MWCNT, (b) N-C-MWCNT, and (c) N-AC-MWCNT. All electrodes have mass loadings of 15 mg cm^{-2}.

of the wetting behavior of N-AC-MWCNT compared to MWCNT (Figure S6, Supporting Information).

Figure 3A compares CVs for MWCNT, N-C-MWCNT, and N-AC-MWCNT electrodes in a three electrode cell. The electrodes showed nearly box-shaped CVs in an aqueous 0.5 M Na_2SO_4 electrolyte in a voltage window from −1.0 to +0.8 V versus SCE. It is important to note that cell voltage in aqueous electrolytes is usually limited by the potential window of water decomposition (1.2 V).[52] However, voltage windows of 1.7−1.8 V in aqueous Na_2SO_4 electrolytes were reported for single activated carbon electrodes.[52,53] It is known that the enlarged voltage window of porous carbon in a neutral Na_2SO_4 electrolyte is attributed to the high overpotential for dihydrogen evolution.[7−9] The box-shaped CVs obtained in different voltage windows (Figure 3B) indicated a possibility of the fabrication of a supercapacitor device, containing two N-AC-MWCNT electrodes. The increase in the scan rate resulted in increasing current (Figure 3C), indicating good capacitive behavior in a voltage window of 1.8 V. Figure 3D compares capacitance versus scan rate dependencies for MWCNT, N-C-MWCNT, and N-AC-MWCNT electrodes with active mass loading of 15 mg cm^{-2}. The N-AC-MWCNT electrodes showed significantly higher capacitance compared to MWCNT and N-C-MWCNT electrodes (Figure 3, Figure S7, Supporting Information). The difference was especially evident (Figure 3D) at scan rates above 50 mV s^{-1}, where N-AC-MWCNT electrodes showed significant improvement in capacitance retention. The N-AC-MWCNT electrodes showed C_m values of 105.4 and 70.5 F g^{-1} at scan rates of 2 and 200 mV s^{-1}, respectively. The relatively high capacitance of N-C-MWCNT at low scan rates is in agreement with the literature data, discussed above, which indicated that N- and S-doped carbon materials show improved capacitive behavior. The higher capacitance N-AC-MWCNT, compared to N-C-MWCNT, can be attributed to significantly higher surface area and better utilization of the N-doped material. The volumetric capacitances were found to be 34.3 and 205.8 F cm^{-3} for MWCNT and AC, respectively.

Figure 4 compares impedance spectroscopy data for MWCNT, N-C-MWCNT, and N-AC-MWCNT electrodes

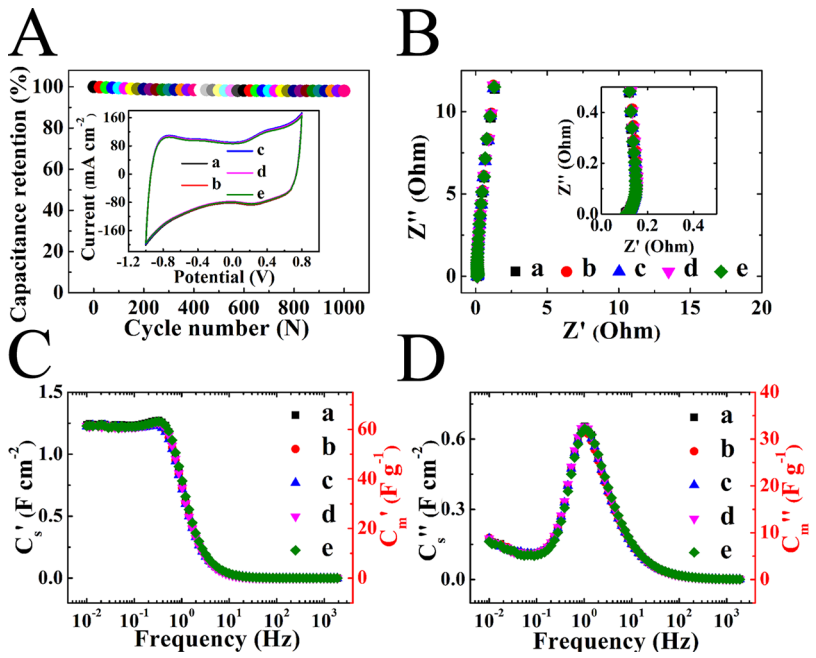

Figure 5. (A) Capacitance retention versus cycle number; inset shows corresponding CVs at 100 mV s^{-1}. (B) Nyquist plot of complex impedance; inset shows high frequency range. (C) C_s' and C_m' and (D) C_s'' and C_m'' versus frequency after (a) 1st, (b) 250th, (c) 500th, (d) 750th, and (e) 1000th cycles for 20 mg cm^{-2} electrodes, prepared from N-AC-MWCNT.

with active mass loadings of 15 mg cm^{-2}. The experimental data presented in the Nyquist plot (Figure 4A) showed relatively low resistance $R = Z'$. The large slope of the Z'' versus Z' curves indicated good capacitive behavior. The analysis of capacitive behavior (Figure 4B,C) showed higher capacitance of N-AC-MWCNT compared to that of MWCNT and N-C-MWCNT. It was found that C' of N-AC-MWCNT was practically frequency independent below 0.7 Hz (Figure 4B). At higher frequencies, a relaxation type of dispersion[54,55] was observed, as indicated by rapid decrease in C' with frequency in the range of 0.7−190 Hz (Figure 4B) and corresponding maximum in the frequency dependence of C'' at 2.1 Hz (Figure 4C). The N-AC-MWCNT showed a relaxation type frequency dispersion of capacitance at much higher frequencies compared to MWCNT and N-C-MWCNT. This indicates improved capacitance retention at high charge−discharge rates in agreement with the results of cyclic voltammetry (Figure 3 and Figure S7, Supporting Information). The improved capacitance behavior of N-AC-MWCNT can be attributed to larger surface area (Figure S1, Supporting Information, Table 1) and better wetting of N-AC-MWCNT by the electrolyte (Figure S6, Supporting Information). It is known that wettability is an important factor, controlling electrochemical performance of carbon electrodes,[56,57] which allows higher capacitance values.

As pointed out above, the fabrication of efficient supercapacitor devices requires good capacitive behavior of electrode materials at high mass loading and high electrode material to current collector mass ratios. Recent reviews[26,56,57] indicated that capacitance of carbon electrodes for aqueous capacitors is typically reported as a mass normalized capacitance (C_m) in KOH or H_2SO_4 electrolytes. However, low materials loading can result in low area normalized capacitance (C_s) at the level[26,56] of 5−15 μF cm^{-2}. It was pointed out[57] that many investigations were limited to relatively low mass loadings. The analysis of C_s data[54] showed that limited electrolyte access to the bulk of thick layers of active material resulted in poor capacitive behavior. Such a bulk layer behaved as a capacitor with low capacitance, connected in series with a capacitive surface layer, and reduced the total capacitance of the electrode. It was shown that high C_m values at low mass loadings do not necessarily indicate good capacitive behavior. It is challenging[57] to achieve good electrochemical performance at materials loading of 10−20 mg cm^{-2}, which is desired for many commercial devices. It is important to note that many investigations of supercapacitor materials involved the fabrication and testing of thin films with mass loadings of 0.005−1 mg cm^{-2}. Such films, deposited on 0.1 mm stainless steel current collectors, have active material to current collector mass ratios in the range from 6.3×10^{-5} to 1.3×10^{-2}. In contrast, in our investigations, the active material loading was in the range of 15−35 mg cm^{-2}, and the active material to current collector mass ratio was in the range of 0.21−0.50. The analysis of experimental data for materials loadings in the range of 15−35 mg cm^{-2} showed very small variations in CV shapes and C_m at low scan rates (Figure S8A,B, Supporting Information). As a result, C_s increased in the range of 1.6−3.6 F cm^{-2} with increasing mass loading (Figure S8C, Supporting Information). The corresponding values of C_m and volume normalized capacitance were 105.4−103.1 F g^{-1} and 38.1−85.7 F cm^{-3}, respectively. However, the increase in mass loading resulted in reduced C_m retention at high scan rates, which was especially evident for material loadings above 25 mg cm^{-2}. The C_m retention at a scan rate of 200 mV s^{-1} was 66.8, 58.7, and 46.0% for material loadings of 15, 25, and 35 mg cm^{-2}, respectively. The corresponding impedance spectroscopy data showed relatively low resistance $R = Z'$ (Figure S8D, Supporting Information). The increase in mass loading resulted in increasing C_s at low frequencies (Figure S8E, Supporting Information) and the shift of the capacitance dispersion to lower frequencies (Figure S8E,F, Supporting Information). The C_s'' maxima were observed at frequencies of 2.0, 0.9, and 0.2

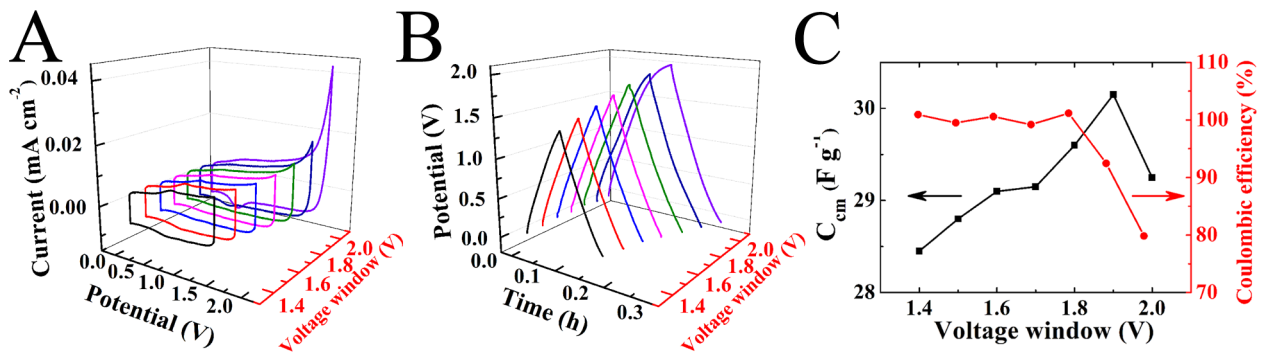

Figure 6. Capacitive behavior for a symmetric cell, containing two N-AC-MWCNT electrodes: (A) CVs at scan rate of 5 mV s^{-1} for different potential windows, (B) charge−discharge curves at a current of 4 mA cm^{-2} for different potential windows, and (C) C_{cm} calculated from charge−discharge curves and Columbic efficiency versus width of the potential window. The mass loadings of individual electrodes is 15 mg cm^{-2}.

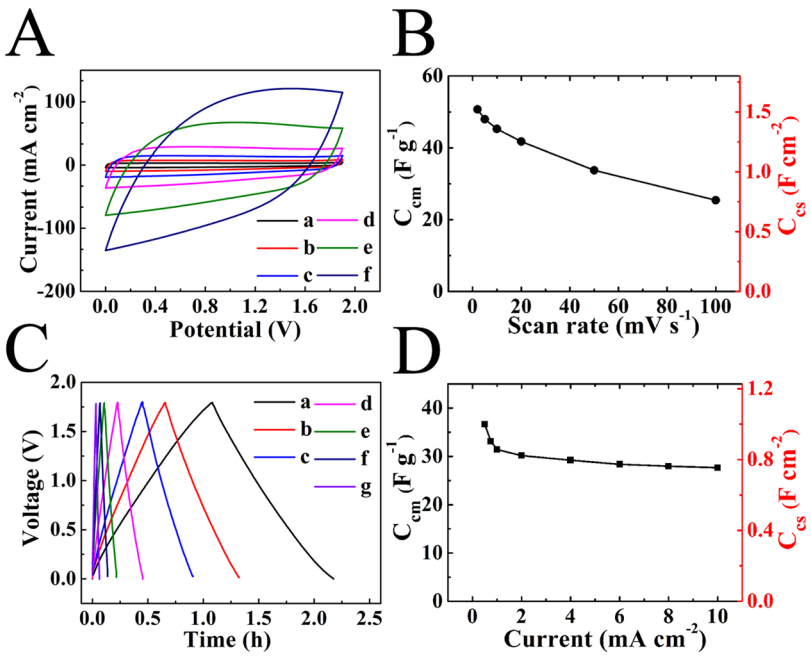

Figure 7. Capacitive behavior of a symmetric cell, containing two N-AC-MWCNT electrodes: (A) CVs at scan rates of (a) 2, (b) 5, (c) 10, (d) 20, (e) 50, and (f) 100 mV s^{-1}. (B) C_{cm} and C_{cs} calculated from CVs versus scan rate. (C) Charge−discharge curves at currents of (a) 0.5, (b) 0.75, (c) 1, (d) 2, (e) 4, (f) 6, and (g) 10 mA cm^{-2}. (D) C_{cm} and C_{cs} calculated from the charge−discharge curves versus current. The mass loading of individual electrodes is 15 mg cm^{-2}.

Hz for mass loadings of 15, 25, and 35 mg cm^{-2}, respectively (Figure S8F, Supporting Information).

The analysis of cyclic stability of individual electrodes in the voltage window of 1.8 V showed that capacitance retention was about 98.0% after 1000 cycles (Figure 5). The analysis of CVs and impedance spectroscopy data did not show significant changes in the CV shape and impedance during cycling. The frequency dependence of AC capacitance remained practically unchanged during cycling (Figure 5C,D).

The individual N-AC-MWCNT electrodes were combined for the fabrication of two-electrode cells. Figure 6(A,B) compares the CV and chronopotentiometry data for supercapacitor cells in different voltage windows. The CV shapes deviated significantly from the ideal box shape for cell voltages above 1.8 V (Figure 6A). The corresponding charge−discharge curves become essentially nonlinear above 1.8 V (Figure 6B). The capacitance C_{cm} increased with increasing cell voltage and showed a maximum at 1.9 V (Figure 6C). The Coulombic efficiency showed very small changes at cell voltages in the range of 1.4−1.8 V and decreased significantly for higher cell voltages. The decrease in the Coulombic efficiency was attributed to electrochemical decomposition of water. Therefore, the cell voltage of 1.8 V was chosen for further investigation of the electrochemical performance of the supercapacitor device.

Figure 7 shows cell testing results for the optimized voltage window of 1.8 V. The cell capacitances C_{cm} and C_{cs}, calculated from the CV data (Figure 7A) decreased from 50.9 to 25.9 F g^{-1} and from 1.54 to 0.77 F cm^{-2} (Figure 7B), respectively, with increasing scan rate from 2 to 100 mV s^{-1}. The cell capacitances, C_{cm} and C_{cs}, calculated from the chronopotentiometry data (Figure 7C) decreased from 36.6 to 27.6 F g^{-1} and 1.0 to 0.76 F cm^{-2} (Figure 7D), respectively, with increasing current from 1 to 10 mA cm^{-2}. The Ragone plot presented in Figure 8A indicates that energy density of 16.1 mWh g^{-1} and power density of 14.4 W g^{-1} were achieved. The insets in Figure 8A show coin cells and LED bulbs powered by the coin cells. The analysis of cycling behavior of the cells showed a

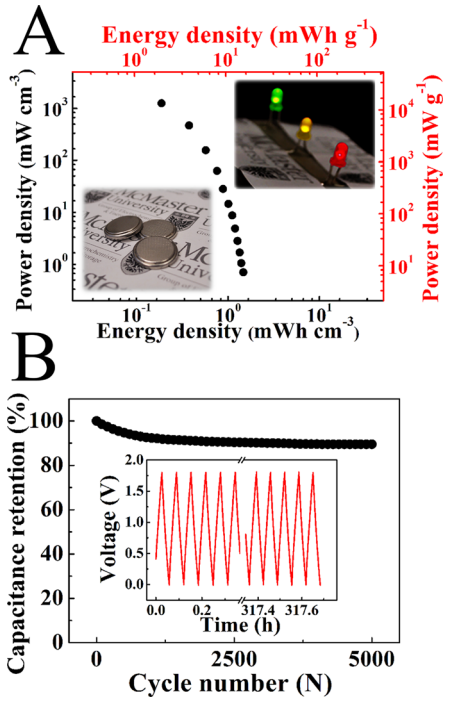

Figure 8. (A) Ragone plot for a coin cell, containing two activated carbon-coated MWCNT electrodes; insets show the coin cells and the light emitting diodes powered by coin cells. (B) Capacitance retention of a coin cell versus cycle number; inset shows the initial and final charge–discharge curves in the cycle performance test.

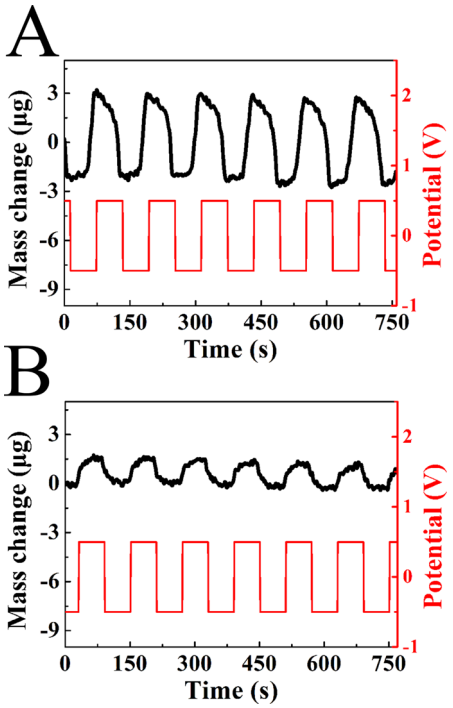

Figure 9. QCM data for mass variation of N-AC-MWCNT-coated resonators during periodic positive and negative pulses with durations of 60 s in (A) 0.05 M Na_2SO_4 and (B) 0.001 M MB dye solutions.

8.1% decrease in the capacitance after 1000 cycles, and then a relatively small decrease in the capacitance was observed (Figure 8B). The capacitance retention after 5000 cycles was 89.5%. The charge–discharge curves were linear and indicated good capacitive behavior (Figure 8B, inset). Impedance studies showed relatively low impedance of the cells (Figure S9, Supporting Information).

The investigation of the self-discharge behavior of the coin cells showed (Figure S10, Supporting Information) an initial voltage drop during 1 h, and then the voltage was nearly constant at the level of 1.2 V during the next 9 h. The N-AC-MWCNT electrodes were also investigated for CDI applications. The ionic fluxes in the N-AC-MWCNT electrodes were analyzed using QCM at reverse pulse conditions (Figure S11, Supporting Information). The investigation of cells, containing a 0.05 M Na_2SO_4 electrolyte (Figure 9A), showed that the application of negative voltage pulses resulted in increasing electrode mass. The increase in the electrode mass resulted from the insertion of Na^+ ions into the N-AC-MWCNT material. The application of the positive current pulses resulted in the mass loss, related to electromigration of Na^+ in the opposite direction. Literature data[58] on QCM analysis of porous electrode materials in periodic electric fields revealed periodic mass gains related to insertion of both cations and anions. However, the QCM studies[59] of CNT electrodes in neutral aqueous solutions showed that a mass gain was observed only when the potential was scanned in the negative direction. Such behavior indicated significant contribution of the cationic transport. Investigations[58−61] demonstrated that relative contributions of cationic and anionic transport to the mass changes of a QCM resonator depend on the relative size of cations and anions and point of zero charge of the electrode material. It was demonstrated that negatively charged carbon nanotubes in aqueous solutions promoted cationic transport.[59] As a result, QCM studies revealed a mass gain only for the negative scans.[59] A similar mechanism can explain the QCM data for N-AC-MWCNT-coated resonators in Na_2SO_4 solutions. The analysis of QCM data for MWCNT-coated resonators showed a similar behavior (Figure S12A, Supporting Information). However, the mass gain for MWCNT was significantly lower compared to that for N-AC-MWCNT. The difference can be attributed to the lower surface area of MWCNT.

The investigations performed in 0.05 M NaCl solutions showed periodic mass gains during negative and positive pulses, corresponding to adsorptions of Na^+ and Cl^- ions, respectively (Figure S13, Supporting Information). The difference in the QCM data for Na_2SO_4 and NaCl solutions indicated that ionic size and charge affect the electrosorption behavior in agreement with the data of other investigations.[58,60−62]

QCM studies showed periodic mass gains during positive pulses for N-AC-MWCNT-coated resonators in the 0.001 M MB dye solutions (Figure 9B). Such mass gains resulted from the insertion of the anionic MB dye into the porous N-AC-MWCNT electrodes. Therefore, the N-AC-MWCNT electrodes can be used for CDR from the dye solutions. In contrast, very small variations in the electrode mass were observed for the MWCNT electrodes (Figure S12B, Supporting Information). The mass variations for MB dye solutions were smaller compared to the mass variations obtained for Na_2SO_4 solutions (Figure 9). The difference can be attributed to larger mass and lower mobility of the MB dyes.

It is important to note that organic dyes are used for many commercial applications.[63] The removal of dyes from the waste solutions is important from the environmental viewpoint because most of the dyes are toxic, mutagenic, and carcinogenic.[64] MB dye was used as a model adsorbate[65−67]

dx.doi.org/10.1021/sc500118r | ACS Sustainable Chem. Eng. 2014, 2, 1289−1298

in order to analyze the efficiency of various adsorbents. It was found that activated carbons are important adsorbents for MB removal.[68,69] The results of our investigation indicated that N-AC-MWCNT is a promising electrode material for MB removal by the CDR method. The use of CDR offers the advantages of high efficiency, energy savings, reversibility, and simple regeneration of the active material.

In the previous studies of electrodes for CDI technology, the ion removal from the solutions was analyzed on the basis of measurements of the electrical conductivity of the solutions.[10,11,13,15−17,19,62] The QCM method used in this investigation addresses the need for in situ analysis of ionic fluxes of charged species in porous electrodes during charge and discharge. The results of our investigation showed that QCM can be used for the investigation of electrosorption and electrodesorption of ions and charged dyes. This method has a high potential for the development of CDI and CDR technologies.

CONCLUSIONS

A new method has been developed for the fabrication of well-dispersed N-AC-MWCNT with high surface area for application in electrodes of electrochemical supercapacitors. The method allowed the fabrication of electrodes with active high mass loading in the range of 15−35 mg cm^{-2} and with a high active material to current collector mass ratio in the range of 0.21−0.50. The highest capacitance of 3.6 F cm^{-2} was achieved in a voltage window of 1.8 V in an aqueous Na_2SO_4 electrolyte. The supercapacitor cells, based on N-AC-MWCNT electrodes, exhibited excellent performance with energy density of 16.1 mWh g^{-1} and power density of 14.4 W g^{-1} in a voltage window of 1.8 V. The individual electrodes and cells showed good capacitance retention at high charge−discharge rates and good cycling stability. The N-AC-MWCNT electrodes showed promising performance for CDI and CDR applications. The QCM method can be used as an efficient tool for the development of electrodes for CDI and CDR technologies.

ASSOCIATED CONTENT

Supporting Information

BET, XRD, Raman spectroscopy data, sedimentation tests, electrochemical testing, and QCM data. This material is available free of charge via the Internet at http://pubs.acs.org.

AUTHOR INFORMATION

Corresponding Author

*Phone: 905-525-9140. E-mail: zhitom@mcmaster.ca.

Notes

The authors declare no competing financial interest.

ACKNOWLEDGMENTS

The authors gratefully acknowledge the financial support of the Natural Sciences and Engineering Research Council of Canada.

REFERENCES

(1) Bose, S.; Kuila, T.; Mishra, A. K.; Rajasekar, R.; Kim, N. H.; Lee, J. H. Carbon-based nanostructured materials and their composites as supercapacitor electrodes. *J. Mater. Chem.* **2012**, *22*, 767−784.

(2) Brousse, T.; Toupin, M.; Belanger, D. A hybrid activated carbon-manganese dioxide capacitor using a mild aqueous electrolyte. *J. Electrochem. Soc.* **2004**, *151*, A614−A622.

(3) Plonska-Brzezinska, M. E.; Echegoyen, L. Carbon nano-onions for supercapacitor electrodes: Recent developments and applications. *J. Mater. Chem. A* **2013**, *1*, 13703−13714.

(4) Cui, X.; Hu, F.; Wei, W.; Chen, W. Dense and long carbon nanotube arrays decorated with Mn_3O_4 nanoparticles for electrodes of electrochemical supercapacitors. *Carbon* **2011**, *49*, 1225−1234.

(5) Khomenko, V.; Raymundo-Piñero, E.; Béguin, F. Optimisation of an asymmetric manganese oxide/activated carbon capacitor working at 2 V in aqueous medium. *J. Power Sources* **2006**, *153*, 183−190.

(6) Gogotsi, Y.; Simon, P. True performance metrics in electrochemical energy storage. *Science* **2011**, *334*, 917−918.

(7) Fic, K.; Frackowiak, E.; Beguin, F. Unusual energy enhancement in carbon-based electrochemical capacitors. *J. Mater. Chem.* **2012**, *22*, 24213−24223.

(8) Gao, Q.; Demarconnay, L.; Raymundo-Piñero, E.; Beguin, F. Exploring the large voltage range of carbon/carbon supercapacitors in aqueous lithium sulfate electrolyte. *Energy Environ. Sci.* **2012**, *5*, 9611−9617.

(9) Demarconnay, L.; Raymundo-Piñero, E.; Béguin, F. A symmetric carbon/carbon supercapacitor operating at 1.6 V by using a neutral aqueous solution. *Electrochem. Commun.* **2010**, *12*, 1275−1278.

(10) Wang, H.; Zhang, D.; Yan, T.; Wen, X.; Zhang, J.; Shi, L.; Zhong, Q. Three-dimensional macroporous graphene architectures as high performance electrodes for capacitive deionization. *J. Mater. Chem. A* **2013**, *1*, 11778−11789.

(11) Li, H.; Liang, S.; Li, J.; He, L. The capacitive deionization behaviour of a carbon nanotube and reduced graphene oxide composite. *J. Mater. Chem. A* **2013**, *1*, 6335−6341.

(12) Wang, H.; Zhang, D.; Yan, T.; Wen, X.; Shi, L.; Zhang, J. Graphene prepared via a novel pyridine−thermal strategy for capacitive deionization. *J. Mater. Chem.* **2012**, *22*, 23745−23748.

(13) Zhang, D.; Yan, T.; Shi, L.; Peng, Z.; Wen, X.; Zhang, J. Enhanced capacitive deionization performance of graphene/carbon nanotube composites. *J. Mater. Chem.* **2012**, *22*, 14696−14704.

(14) El-Deen, A. G.; Barakat, N. A.; Khalil, K. A.; Kim, H. Y. Development of multi-channel carbon nanofibers as effective electrosorptive electrodes for a capacitive deionization process. *J. Mater.Chem. A* **2013**, *1*, 11001−11010.

(15) Wen, X.; Zhang, D.; Yan, T.; Zhang, J.; Shi, L. Three-dimensional graphene-based hierarchically porous carbon composites prepared by a dual-template strategy for capacitive deionization. *J. Mater.Chem. A* **2013**, *1*, 12334−12344.

(16) Yan, C.; Zou, L.; Short, R. Single-walled carbon nanotubes and polyaniline composites for capacitive deionization. *Desalination* **2012**, *290*, 125−129.

(17) Zhang, D.; Wen, X.; Shi, L.; Yan, T.; Zhang, J. Enhanced capacitive deionization of graphene/mesoporous carbon composites. *Nanoscale* **2012**, *4*, 5440−5446.

(18) Porada, S.; Borchardt, L.; Oschatz, M.; Bryjak, M.; Atchison, J.; Keesman, K.; Kaskel, S.; Biesheuvel, P.; Presser, V. Direct prediction of the desalination performance of porous carbon electrodes for capacitive deionization. *Energy Environ. Sci.* **2013**, *6*, 3700−3712.

(19) Yang, J.; Zou, L.; Choudhury, N. R. Ion-selective carbon nanotube electrodes in capacitive deionisation. *Electrochim. Acta* **2013**, *91*, 11−19.

(20) Goh, P.; Ismail, A.; Ng, B. Carbon nanotubes for desalination: Performance evaluation and current hurdles. *Desalination* **2012**, *308*, 2−14.

(21) Simon, P.; Gogotsi, Y. Materials for electrochemical capacitors. *Nat. Mater.* **2008**, *7*, 845−854.

(22) Cao, Z.; Wei, B. A perspective: Carbon nanotube macro-films for energy storage. *Energy Environ. Sci.* **2013**, *6*, 3183−3201.

(23) Frackowiak, E.; Abbas, Q.; Beguin, F. Carbon/carbon supercapacitors. *J. Energy Chem.* **2013**, *22*, 226−240.

(24) Vilatela, J. J.; Eder, D. Nanocarbon composites and hybrids in sustainability: A review. *ChemSusChem* **2012**, *5*, 456−478.

(25) Jiang, H.; Lee, P. S.; Li, C. 3D carbon based nanostructures for advanced supercapacitors. *Energy Environ.Sci.* **2012**, *6*, 41−53.

(26) Obreja, V. V. N. On the performance of supercapacitors with electrodes based on carbon nanotubes and carbon activated material—A review. *Phys. E* **2008**, *40*, 2596–2605.
(27) Zhi, M.; Xiang, C.; Li, J.; Li, M.; Wu, N. Nanostructured carbon-metal oxide composite electrodes for supercapacitors: A review. *Nanoscale* **2013**, *5*, 72–88.
(28) Gu, W.; Sevilla, M.; Magasinski, A.; Fuertes, A. B.; Yushin, G. Sulfur-containing activated carbons with greatly reduced content of bottle neck pores for double-layer capacitors: a case study for pseudocapacitance detection. *Energy Environ. Sci.* **2013**, *6*, 2465–2476.
(29) Chen, L.-F.; Huang, Z.-H.; Liang, H.-W.; Yao, W.-T.; Yu, Z.-Y.; Yu, S.-H. Flexible all-solid-state high-power supercapacitor fabricated with nitrogen-doped carbon nanofiber electrode material derived from bacterial cellulose. *Energy Environ. Sci.* **2013**, *6*, 3331–3338.
(30) Chen, L.-F.; Zhang, X.-D.; Liang, H.-W.; Kong, M.; Guan, Q.-F.; Chen, P.; Wu, Z.-Y.; Yu, S.-H. Synthesis of nitrogen-doped porous carbon nanofibers as an efficient electrode material for supercapacitors. *ACS Nano* **2012**, *6*, 7092–7102.
(31) Kim, W.; Kang, M. Y.; Joo, J. B.; Kim, N. D.; Song, I. K.; Kim, P.; Yoon, J. R.; Yi, J. Preparation of ordered mesoporous carbon nanopipes with controlled nitrogen species for application in electrical double-layer capacitors. *J. Power Sources* **2010**, *195*, 2125–2129.
(32) Zhou, D.-D.; Li, W.-Y.; Dong, X.-L.; Wang, Y.-G.; Wang, C.-X.; Xia, Y.-Y. A nitrogen-doped ordered mesoporous carbon nanofiber array for supercapacitors. *J. Mater. Chem. A* **2013**, *1*, 8488–8496.
(33) Hulicova-Jurcakova, D.; Seredych, M.; Lu, G. Q.; Bandosz, T. J. Combined effect of nitrogen- and oxygen-containing functional groups of microporous activated carbon on its electrochemical performance in supercapacitors. *Adv. Funct. Mater.* **2009**, *19*, 438–447.
(34) Song, Y.; Zhou, D.; Wang, Y.; Wang, C.; Xia, Y. Preparation of nitrogen-containing mesoporous carbons and their application in supercapacitors. *New J. Chem.* **2013**, *37*, 1768–1775.
(35) Wei, L.; Sevilla, M.; Fuertes, A. B.; Mokaya, R.; Yushin, G. Polypyrrole-derived activated carbons for high-performance electrical double-layer capacitors with ionic liquid electrolyte. *Adv. Funct. Mater.* **2012**, *22*, 827–834.
(36) Li, L.; Liu, E.; Li, J.; Yang, Y.; Shen, H.; Huang, Z.; Xiang, X.; Li, W. A doped activated carbon prepared from polyaniline for high performance supercapacitors. *J. Power Sources* **2010**, *195*, 1516–1521.
(37) Qie, L.; Chen, W.; Xu, H.; Xiong, X.-Q.; Jiang, Y.; Zou, F.; Hu, X.; Xin, Y.; Zhang, Z.; Huang, Y. Synthesis of functionalized 3D hierarchical porous carbon for high-performance supercapacitor. *Energy Environ. Sci.* **2013**, *6*, 2497–2504.
(38) Guo, C.; Li, N.; Ji, L.; Li, Y.; Yang, X.; Lu, Y.; Tu, Y. N-and O-doped carbonaceous nanotubes from polypyrrole for potential application in high-performance capacitance. *J. Power Sources* **2014**, *247*, 660–666.
(39) Wang, Z.; Qie, L.; Yuan, L.; Zhang, W.; Hu, X.; Huang, Y. Functionalized N-doped interconnected carbon nanofibers as an anode material for sodium-ion storage with excellent performance. *Carbon* **2013**, *55*, 328–334.
(40) Qie, L.; Chen, W.-M.; Wang, Z.-H.; Shao, Q.-G.; Li, X.; Yuan, L.-X.; Hu, X.-L.; Zhang, W.-X.; Huang, Y.-H. Nitrogen-doped porous carbon nanofiber webs as anodes for lithium ion batteries with a superhigh capacity and rate capability. *Adv. Mater.* **2012**, *24*, 2047–2050.
(41) Wang, H.-g.; Wu, Z.; Meng, F.-l.; Ma, D.-l.; Huang, X.-l.; Wang, L.-m.; Zhang, X.-b. Nitrogen-doped porous carbon nanosheets as low-cost, high-performance anode material for sodium-ion batteries. *ChemSusChem* **2013**, *6*, 56–60.
(42) Shi, K.; Zhitomirsky, I. Fabrication of polypyrrole-coated carbon nanotubes using oxidant-surfactant nanocrystals for supercapacitor electrodes with high mass loading and enhanced performance. *ACS Appl. Mater. Interfaces* **2013**, *5*, 13161–13170.
(43) Wu, T.; Liu, G.; Zhao, J.; Hidaka, H.; Serpone, N. Evidence for H_2O_2 generation during the TiO_2-assisted photodegradation of dyes in aqueous dispersions under visible light illumination. *J. Phys. Chem. B* **1999**, *103*, 4862–4867.
(44) Chen, C.; Ma, W.; Zhao, J. Semiconductor-mediated photodegradation of pollutants under visible-light irradiation. *Chem. Soc. Rev.* **2010**, *39*, 4206–4219.
(45) Chen, Y.; Huang, R.; Chen, D.; Wang, Y.; Liu, W.; Li, X.; Li, Z. Exploring the different photocatalytic performance for dye degradations over hexagonal ZnIn2S4 microspheres and cubic $ZnIn_2S_4$ Nanoparticles. *ACS Appl. Mater. Interfaces* **2012**, *4*, 2273–2279.
(46) Zhang, W.; Yang, Z.; Wang, X.; Zhang, Y.; Wen, X.; Yang, S. Large-scale synthesis of β-MnO_2 nanorods and their rapid and efficient catalytic oxidation of methylene blue dye. *Catal. Commun.* **2006**, *7*, 408–412.
(47) Yuan, J.; Liu, X.; Akbulut, O.; Hu, J.; Suib, S. L.; Kong, J.; Stellacci, F. Superwetting nanowire membranes for selective absorption. *Nat. Nanotechnol.* **2008**, *3*, 332–336.
(48) Wu, J.; Wang, J.; Li, H.; Du, Y.; Huang, K.; Liu, B. Designed synthesis of hematite-based nanosorbents for dye removal. *J. Mater. Chem. A* **2013**, *1*, 9837–9847.
(49) Deakin, M. R.; Buttry, D. A. Electrochemical applications of the quartz crystal microbalance. *Anal. Chem.* **1989**, *61*, 1147A–1154A.
(50) Sauerbrey, G. Verwendung von Schwingquarzen zur Wägung dünner Schichten und zur Mikrowägung. *Z. Phys. A: Hadrons Nucl.* **1959**, *155*, 206–222.
(51) Yang, M.; Cheng, B.; Song, H.; Chen, X. Preparation and electrochemical performance of polyaniline-based carbon nanotubes as electrode material for supercapacitor. *Electrochim. Acta* **2010**, *55*, 7021–7027.
(52) Wu, T.-H.; Hsu, C.-T.; Hu, C.-C.; Hardwick, L. J. Important parameters affecting the cell voltage of aqueous electrical double-layer capacitors. *J. Power Sources* **2013**, *242*, 289–298.
(53) Hsu, Y.-K.; Chen, Y.-C.; Lin, Y.-G.; Chen, L.-C.; Chen, K.-H. High-cell-voltage supercapacitor of carbon nanotube/carbon cloth operating in neutral aqueous solution. *J. Mater. Chem.* **2012**, *22*, 3383–3387.
(54) Shi, K.; Zhitomirsky, I. Influence of current collector on capacitive behavior and cycling stability of Tiron doped polypyrrole electrodes. *J. Power Sources* **2013**, *240*, 42–49.
(55) Shi, K.; Zhitomirsky, I. Polypyrrole nanofiber-carbon nanotube electrodes for supercapacitors with high mass loading obtained using an organic dye as a co-dispersant. *J. Mater. Chem. A* **2013**, *1*, 11614–11622.
(56) Zhang, L. L.; Gu, Y.; Zhao, X. S. Advanced porous carbon electrodes for electrochemical capacitors. *J. Mater. Chem. A* **2013**, *1*, 9395–9408.
(57) Wei, L.; Yushin, G. Nanostructured activated carbons from natural precursors for electrical double layer capacitors. *Nano Energy* **2012**, *1*, 552–565.
(58) Levi, M. D.; Salitra, G.; Levy, N.; Aurbach, D.; Maier, J. Application of a quartz-crystal microbalance to measure ionic fluxes in microporous carbons for energy storage. *Nat. Mater.* **2009**, *8*, 872–875.
(59) Barisci, J. N.; Wallace, G. G.; Baughman, R. H. Electrochemical quartz crystal microbalance studies of single-wall carbon nanotubes in aqueous and non-aqueous solutions. *Electrochim. Acta* **2000**, *46*, 509–517.
(60) Sigalov, S.; Levi, M. D.; Salitra, G.; Aurbach, D.; Maier, J. EQCM as a unique tool for determination of ionic fluxes in microporous carbons as a function of surface charge distribution. *Electrochem. Commun.* **2010**, *12*, 1718–1721.
(61) Levy, N.; Levi, M. D.; Aurbach, D.; Demadrille, R.; Pron, A. Failure and stabilization mechanisms in multiply cycled conducting polymers for energy storage devices. *J. Phys. Chem. C* **2010**, *114*, 16823–16831.
(62) Gabelich, C. J.; Tran, T. D.; Suffet, I. H. Electrosorption of inorganic salts from aqueous solution using carbon aerogels. *Environ. Sci. Technol.* **2002**, *36*, 3010–3019.
(63) Bulut, Y.; Aydin, H. A kinetics and thermodynamics study of methylene blue adsorption on wheat shells. *Desalination* **2006**, *194*, 259–267.

(64) Pavan, F. A.; Lima, E. C.; Dias, S. L.; Mazzocato, A. C. Methylene blue biosorption from aqueous solutions by yellow passion fruit waste. *J. Hazard. Mater.* **2008**, *150*, 703−712.
(65) Wang, S.; Gao, Q.; Luo, W. J.; Xu, J.; Zhou, C. G.; Xia, H. Removal of methyl blue from aqueous solution by magnetic carbon nanotube. *Water Sci. Technol.* **2013**, *68*, 665−673.
(66) Zhang, F.; Zhao, Z.; Tan, R.; Guo, Y.; Cao, L.; Chen, L.; Li, J.; Xu, W.; Yang, Y.; Song, W. Selective and effective adsorption of methyl blue by barium phosphate nano-flake. *J. Colloid Interface Sci.* **2012**, *386*, 277−284.
(67) Wu, T.; Cai, X.; Tan, S.; Li, H.; Liu, J.; Yang, W. Adsorption characteristics of acrylonitrile, p-toluenesulfonic acid, 1-naphthalenesulfonic acid and methyl blue on graphene in aqueous solutions. *Chem. Eng. J.* **2011**, *173*, 144−149.
(68) Tseng, R.-L.; Wu, P.-H.; Wu, F.-C.; Juang, R.-S. Half-life and half-capacity concentration approach for the adsorption of 2,4-dichlorophenol and methyl blue from water on activated carbons. *J. Taiwan Inst. Chem. Eng.* **2011**, *42*, 312−319.
(69) Iqbal, M. J.; Ashiq, M. N. Adsorption of dyes from aqueous solutions on activated charcoal. *J. Hazard. Mater.* **2007**, *139*, 57−66.